Pseudopotential calculations of band gaps and band edges of short-period $(InAs)_n/(GaSb)_m$ superlattices with different substrates, layer orientations, and interfacial bonds

Paulo Piquini* and Alex Zunger
National Renewable Energy Laboratory, Golden, Colorado 80401, USA

Rita Magri
CNR-INFM-S3 and Dipartimento di Fisica, Università di Modena e Reggio Emilia, Via Campi 213/A, I-41100 Modena, Italy

(Received 8 October 2007; published 12 March 2008)

The band edges and band gaps of $(InAs)_n/(GaSb)_m$ $(n,m=1,20)$ superlattices have been theoretically studied through the plane-wave empirical pseudopotential method for different situations: (i) different substrates, GaSb and InAs; (ii) different point group symmetries, C_{2v} and D_{2d}; and (iii) different growth directions, (001) and (110). We find that (a) the band gaps for the (001) C_{2v} superlattices on a GaSb substrate exhibit a nonmonotonic behavior as a function of the GaSb barrier thickness when the number of $(InAs)_n$ layers exceed $n=5$; (b) substrate effects: compared with the GaSb substrate, the different strain field generated by the InAs substrate leads to a larger variation of the band gaps for the (001) C_{2v} superlattices as a function of the InAs well thickness; (c) effect of the type of interfacial bonds: the In-Sb bonds at the interfaces of the (001) D_{2d} superlattices partially pin the band edge states, reducing the influence of the confinement effects on electrons and holes, and lowering the band gaps as compared to the (001) C_{2v} case. The valence band maximum of the (001) D_{2d} superlattices with Ga-As bonds at the interfaces are shifted down, increasing the band gaps as compared to the (001) C_{2v} case; (d) effect of layer orientation: the presence of In-Sb bonds at both interfaces of the (110) superlattices pin the band edge states and reduces the band gaps, as compared to the (001) C_{2v} case. An anticrossing between the electron and hole levels in the (110) superlattices, for thin GaSb and thick InAs layers, leads to an increase of the band gaps, as a function of the InAs thickness; (e) superlattices vs random alloys: the comparison between the band edges and band gaps of the superlattices on a GaSb substrate and those for random alloys, lattice matched to a GaSb substrate, as a function of the In composition, shows that the random alloys present almost always higher band gaps and give a clear indication of the effect of superlattice's ordering and period on the behavior of the band gaps and band edges. Inclusion of interfacial interdiffusion, using the approach of Magri and Zunger [Phys. Rev. B **65**, 165302 (2002)], is shown to significantly increase the band gaps relative to the predictions for abrupt superlattices, bringing the results closer to experiment. It is noteworthy that $\mathbf{k}\cdot\mathbf{p}$ model fit instead measured gaps corresponding to interdiffused interfaces using a chemically abrupt model.

DOI: 10.1103/PhysRevB.77.115314 PACS number(s): 73.21.Cd, 73.43.Cd, 71.15.Dx

I. INTRODUCTION

Quaternary alloys such as (Ga,In)(As,Sb) or (Ga,In)(As,N), made of two cations and two anions, manifest compositional variability in both sublattices, leading to interesting physical characteristics that are absent in pseudobinary alloys such as (Ga,In)As. Three effects are noteworthy.

(i) *Lattice matching in full composition range.* Unlike pseudobinary alloys, such as $In_xGa_{1-x}As$, which can be lattice matched to a given substrate only for a single composition x, the quaternary $In_xGa_{1-x}As_ySb_{1-y}$ alloy can lattice match to a given substrate as for many (x,y) values simply by changing simultaneously x and y according to a specific algebraic relationship. For example, lattice matching of the $In_xGa_{1-x}As_ySb_{1-y}$ random alloys to GaSb demands $y=0.001+0.648x+0.239x^2$, whereas lattice matching to InAs requires $y=0.086+0.656x+0.256x^2$.[1] Thus, good quality films can be grown on numerous substrates in the full composition range.

(ii) *Transition from negative to positive band gap as a function of layer thicknesses.* As illustrated in Fig. 1, the InAs/GaSb heterostructure has a broken-gap band alignment, with the InAs conduction band minimum lying

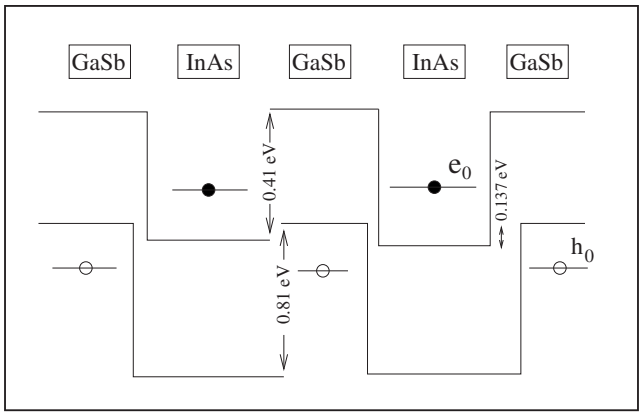

FIG. 1. Schematic figure showing the broken-gap band alignment between the InAs and GaSb layers strained on a GaSb(001) substrate. The electron (filled circles) and hole (empty circles) levels are the confined states of the superlattice, when the InAs and GaSb layers are short enough to open a semiconducting gap due to quantum confinement effects.

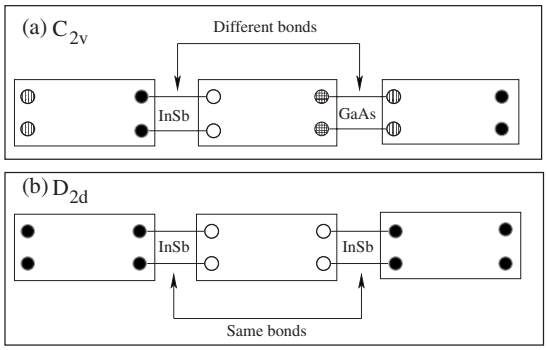

FIG. 2. Schematic illustration of the bond configurations at the interfaces between InAs and GaSb layers in (InAs)/(GaSb) superlattices with C_{2v} and D_{2d} point group symmetries, grown along the (001) direction. In the C_{2v} case, one interface has Ga-As bonds whereas the other has In-Sb bonds. In the D_{2d} case both interfaces have the same bond type: either both Ga-As or both In-Sb.

~150 meV below the GaSb valence band maximum.[2] For short-period $(InAs)_n/(GaSb)_m$ superlattices, quantum confinement pushes up the electron level, e_0, confined within the InAs layers, whereas the hole level, h_0, confined in the GaSb layers is pushed down. This opens an e_0-h_0 semiconducting gap, whose magnitude depends on the layer thicknesses.[3] Hence, the band gaps of the $(InAs)_n/(GaSb)_m$ superlattices can be tailored over a wide range of wavelengths, from the mid-infrared to the very-long-infrared regions, making these materials suitable for optoelectronic devices.[4–14] Note, however, that although the type-II broken-gap band alignment of the InAs/GaSb heterojunctions imply, at first sight, in a semimetallic behavior of these heterostructures, it has been theoretically shown[15–20] and experimentally observed[21] that a hybridization gap is opened due to an anticrossing between the electron and hole levels for certain k vectors in the in-plane direction.

(iii) *Different types of interfacial bonds in the (001) superlattices depending on the point group symmetry.* Unlike common atom pseudobinaries, such as (Ga,In)As, which have two types of bonds, In-As and Ga-As, the non-common-atom quaternary alloys, such as (Ga,In)(As,Sb), present four types of bonds. In particular, the interfaces between the InAs and GaSb layers in an $(InAs)_n/(GaSb)_m$ (001) superlattice can have either In-Sb or Ga-As bonds (when the number of monolayers in both InAs and GaSb layers is half-integer) or both kind of bonds (when the number of monolayers in InAs and GaSb are integers). Figure 2 indicates that when the bonds at the interfaces are equal, the superlattice point group symmetry will be the same as in the common-atom pseudobinaries, namely, D_{2d}. However, if the bonds at the interfaces alternate from In-Sb to Ga-As, the point group symmetry reduces to C_{2v}. This difference has important consequences for the optoelectronic properties of the C_{2v} superlattices,[22–24] showing an in-plane polarization anisotropy[25] and the appearance of otherwise parity forbidden transitions.[26]

The use of $(InAs)_n/(GaSb)_m$ superlattices for mid-infrared lasers and photodetectors depends on the accurate design of their band gaps and the successful growth of these superlattices. Some factors that can influence the final band gaps for these superlattices include (i) the InAs and GaSb layer thicknesses, (ii) the point group symmetries resulting from the type of bonds at the interfaces, (iii) the choice of substrate, and (iv) the layer orientation. Previous theoretical efforts focusing on band gaps of these superlattices have concentrated mainly on (001) $(InAs)_n/(GaSb)_m$ superlattices grown on GaSb substrates with either C_{2v} or D_{2d} (with In-Sb bonds at the interfaces) point group symmetry, for some set of the n and m values.[17,24,27] In the present work, we study the effect of different factors on the behavior of the band edges and band gaps of the $(InAs)_n/(GaSb)_m$ superlattices with abrupt interfaces, for n and m varying from 1 to 20. We first present, as reference, the results for the C_{2v} (001) superlattices grown on a GaSb substrate, and then we analyze the influences of different substrates, different point group symmetries, and different growing directions. In addition, we compare the results for the superlattices grown on GaSb substrates with those for random alloys with equivalent In composition. This allows a broad view of the configurational space available for the design of $(InAs)_n/(GaSb)_m$ short-period superlattices suitable for applications in mid- and long-infrared active devices.

The $(InAs)_n/(GaSb)_m$ superlattices are known to have interfaces that are not always abrupt, but show some atomic concentration profiles due to the tendency of the As and Sb atoms to intermix.[28] These atomic concentration profiles along the growth direction can influence the absolute values of the band gaps.[23,29,30] An accurate prediction of the specific band gap and band edge values should take the corrections due to atomic segregation into account. We calculate the segregation profiles for some selected superlattices and show that it increases the band gap values, as compared with those for the abrupt interfaces, leading to a much better agreement with experimental values.

II. METHOD OF CALCULATION

The study of the $(InAs)_n/(GaSb)_m$ $(n,m=1,20)$ superlattices on different substrates (InAs and GaSb), with different point group symmetries (D_{2d} and C_{2v}) and at different layer orientations [(001) and (110)], as well as the random alloys for different In compositions comprises more than 2000 different configurations. The number of atoms in the supercells used to study the superlattices varies from 8 to 320, whereas the supercells for the random alloys contain 512 atoms.

Ab initio approaches based on the local density or the generalized gradient approximations to the exchange and correlation potential of the density functional theory are known to underestimate the gap values by as much as 50%.[31] Even worse, local density approximation (LDA) underestimates greatly the effective masses,[32,33] which is detrimental to quantitative prediction of quantum confinement. Also, the use of *ab initio* methods to treat the random alloy samples would be costly, due to the large number of atoms that are required in the supercell in order to approach a random distribution of the atoms.

The standard $\mathbf{k}\cdot\mathbf{p}$-based envelope function approximation (EFA) methods, on the other hand, produce results at a low

computational cost. In these methods, the wave functions of the system are expanded in a basis set built from only Γ-like Bloch functions of the parent bulk materials.[34,35] If the basis set is complete (all bands) the method would be in principle exact (provided that interface related features are correctly taken into account).[36] In practice $\mathbf{k}\cdot\mathbf{p}$ EFA calculations employ a small basis set, with the most common approximations involving just the bands at the top of the valence band (the 6×6 $\mathbf{k}\cdot\mathbf{p}$ model), or including additionally the states at the bottom of the conduction band (the 8×8 model). The incompleteness of the truncated basis set is then mitigated by adjusting the model parameters to match the available experimental data. This procedure works well for bulk phases or wide quantum wells. However, when the dimensionality of the system is reduced, and the symmetry of the system departs significantly from that of the parent bulk materials from which the basis functions are drawn, these approaches fail to provide a correct description of the system's properties. We first indicate some of the *qualitative* failures often referred to as the "farsightedness of $\mathbf{k}\cdot\mathbf{p}$."[37] For example, Wang *et al.*[3] showed, through a direct comparison between plane-wave pseudopotential and the 8×8 $\mathbf{k}\cdot\mathbf{p}$ approach, that the $\mathbf{k}\cdot\mathbf{p}$ fails qualitatively in describing both the electron–heavy-hole coupling and the light-hole–heavy-hole coupling and anticrossing in InAs/GaSb superlattices, and consequently misses altogether the strong in-plane polarization anisotropy of the interband transitions. Also, Magri and Zunger[38] showed that the $\mathbf{k}\cdot\mathbf{p}$ model misses the correct D_{2d} symmetry for GaAs/Al_xGa_{1-x}As heterostructures and thus incorrectly predicts zero coupling between the odd-parity light-hole states and the even-parity heavy-hole states at the zone center. Fu *et al.*[39] studied spherical quantum dots of CdSe and InP using 6×6 and 8×8 $\mathbf{k}\cdot\mathbf{p}$ as well as plane-wave atomistic pseudopotential approaches. They found that the 6×6 model predicts an incorrect energetic order of the highest valence *s* and *p* states for both kinds of dots and fails to show the *L* character of the second conduction state in the Brillouin zone, incorrectly predicting all states as having a Γ-like character. Similar failure of $\mathbf{k}\cdot\mathbf{p}$ in missing numerous hole states in the top ≃300 meV range below the valence band maximum (VBM) of CdSe (Ref. 39) and PbSe.[40] Kim *et al.*[41] used the pseudopotential plane-wave approach to study the electronic structure of strained InAs pyramidal quantum dots embedded in a GaAs matrix. They found up to six bound electron states (without spin degeneracy) in the dots, which is in clear contrast with $\mathbf{k}\cdot\mathbf{p}$ calculations,[42] which predicts only one bound electron state for the same system. As to *quantitative* failures, Ref. 43 lists the relative energy shifts of $\mathbf{k}\cdot\mathbf{p}$ vs pseudopotential for the *same* system of InAs/GaAs dots whereas Refs. 39 and 40 list them for CdSe and PbSe, respectively. These and other results for heterostructures[16,44,45] and quantum dots[46–51] show that the application of the standard EFA model to short-period superlattices is not completely justified. Szmulowicz *et al.*[24] fixed some of the $\mathbf{k}\cdot\mathbf{p}$ deficiencies by introducing *ad hoc* an adjustable potential centered at the interfaces[52] in order to consider the symmetry of the superlattices with non-common atom interfaces. The value of this added potential is not established by the $\mathbf{k}\cdot\mathbf{p}$ theory itself but must be imported from other types of theory or from fitting some experiments. The interfaces remain abrupt.

An atomistic description of the interface structure as well as of the atomic potentials and chemical bonds is crucial to describe the details of the electronic structure of superlattices, in particular, the short-period non-common-atom superlattices as the $(InAs)_n/(GaSb)_m$ ones. The methodology employed to study the $(InAs)_n/(GaSb)_m$ short-period superlattices in this work, the plane-wave empirical pseudopotential method, is capable to correctly describe the atomistic structure of the superlattices, taking automatically into account the underlying symmetries derived by the different growing directions and different kinds of interface bonds, while maintaining the computational cost relatively low.

A. Structural relaxation

We have constrained all superlattices and alloys to have the in-plane lattice constants of a specific substrate (GaSb or InAs). Such epitaxial conditions lead to compressive or tensile strain fields in the perpendicular direction. The corresponding strain relaxation and atomic optimization have been performed through the valence force field (VFF) method,[45,53,54] by minimizing the strain energy along the growth direction. The VFF strain energy, E_{strain}, is expressed as

$$E_{strain} = \sum_i \sum_j^{\mathrm{NN}_i} \frac{3}{8}\frac{\alpha_{ij}}{(d_{ij}^0)^2}[(\mathbf{R}_j-\mathbf{R}_i)^2-(d_{ij}^0)^2]^2 + \sum_i \sum_{k>j}^{\mathrm{NN}_i} \left\{ \frac{3}{8}\frac{\beta_{ijk}}{d_{ij}^0 d_{ik}^0}[(\mathbf{R}_i-\mathbf{R}_j)\cdot(\mathbf{R}_k-\mathbf{R}_i) - d_{ij}^0 d_{ik}^0 \cos(\theta_{ijk}^0)]^2 \right\}, \quad (1)$$

where $\mathbf{R}_i$ is the position vector of atom *i*, and the d_{ij}^0 represents the ideal interatomic distance between atoms *i* and *j* in the respective binary. The NN_i means that the sums run over the nearest neighbor atoms. Here, α_{ij} and β_{ijk} are force constants fitted to reproduce elastic constants of pure binary materials. The VFF is known to accurately reproduce the elastic energies as obtained by LDA for InAs buried layers in a GaAs host,[55] various $(InP)_n/(GaP)_m$ superstructures,[56] and III-V nitrides.[57]

B. Single-particle equations and potentials

Once the relaxed atomic coordinates and lattice constants are obtained, the electronic structure is evaluated solving the effective single-particle Schrödinger equation

$$\left\{-\frac{\beta}{2}\nabla^2+V_{ps}\right\}\psi_i(\mathbf{r})=\epsilon_i\psi_i(\mathbf{r}), \quad (2)$$

where V_{ps}, the pseudopotential, is written as

$$V_{ps}=\sum_{\alpha,n} v_\alpha(\mathbf{r}-\mathbf{R}_n-\mathbf{d}_\alpha), \quad (3)$$

with v_α representing the screened atomic pseudopotential of atom α (In, Ga, As, or Sb) located at the site $\mathbf{d}_\alpha$ within the unit cell designated by the lattice vector $\mathbf{R}_n$. These screened

atomic pseudopotentials are described through a strain-dependent continuous analytic function of momentum $\mathbf{q}$, whose parameters are adjusted to reproduce calculated and measured[58] properties of the four binaries (InAs, InSb, GaAs, and GaSb) and their possible ternary (or pseudobinary) compounds.[1,23] The target properties are the band gaps; the eigenvalues at the L, X, and Γ points; the effective masses; the deformation potentials; the spin-orbit splitting; and the valence band offsets. The multiplying factor β in Eq. (1) is a scaling parameter for the kinetic energy that recovers, to a first order approximation, the contributions due to the self-energy.[59] The expression of the strain-dependent screened atomic pseudopotential is given by[45]

$$v_\alpha(q,\epsilon) = v_\alpha(q,0)[1 + \gamma_\alpha \mathrm{Tr}(\epsilon)], \tag{4}$$

where γ_α is a strain related parameter and $\mathrm{Tr}(\epsilon)$ is the trace of the strain tensor, ϵ, calculated through the VFF method.

C. Wave function expansion and solutions of the electronic problem

The wave functions ψ_i in Eq. (2) are expanded in terms of plane waves, with a cutoff energy of 5 Ry (determined at the stage when the pseudopotential V_{ps} is generated). The diagonalization of the Hamiltonian in Eq. (1) is performed via the folded spectrum method,[60] in which the Schrödinger equation is transformed into a quadratic form, according to

$$(\hat{H} - \epsilon_{ref})^2 \psi_i = (\epsilon - \epsilon_{ref})^2 \psi_i, \tag{5}$$

and the problem is solved for a chosen number of eigenvalues that are the closest, in absolute values, to the given reference energy, ϵ_{ref}. Thus, once one is interested in the eigenvalues within a certain energy range (the gap region, for example), the diagonalization of the expectation value of the Schrödinger Hamiltonian for the complete set of occupied single-particle orbitals can be circumvented, reducing enormously the computational effort without losing accuracy.

III. (001) $(InAs)_n/(GaSb)_m$ C_{2v} SUPERLATTICES ON A GaSb SUBSTRATE

We determined the band gaps and band edges of the (001) $(InAs)_n/(GaSb)_m$ $(n,m=1,20)$ superlattices with C_{2v} point group symmetry on a GaSb substrate. The calculated lowest confined electron state [the conduction band minimum (CBM)] and the first confined hole state [the valence band maximum (VBM)] eigenvalues for 400 different superlattices are shown in Figs. 3(a) and 3(c), respectively, as a function of the number of GaSb layers in the superlattices. Each different curve represents a different InAs layer thickness.

A. Band edges

The general trends of the CBM and VBM eigenvalues can be analyzed within two different regimes.

(1) Regime I—Interacting quantum wells (QW's): thin GaSb layers

In this regime we see from Figs. 3(a) and 3(c) the following.

(i) The superlattice CBM shows a redshift with decreasing GaSb thickness: This occurs because the level repulsion between the electron levels in adjacent InAs wells shifts down the CBM level.

(ii) For increasing InAs thickness, the superlattice CBM tends to the CBM of the strained bulk InAs: This happens because of the reduction in intensity of the confinement effect for increasing InAs width, which pushes down the superlattice CBM toward the CBM of the InAs strained bulk.

(iii) For decreasing number of GaSb layers, the superlattice VBM shows a redshift: This occurs because the confinement effect on the hole levels, localized in the GaSb barrier region, increases when the GaSb layer turns thinner.

(iv) For increasing number of InAs layers, a redshift of the superlattice VBM is observed: This is because the overlap of the hole's wave functions in adjacent GaSb barriers diminishes when the InAs wells turn thicker, reducing the upshift of the hole levels due to level repulsion.

(2) Regime II—Toward an isolated QW regime: thick GaSb layers

In this regime we see from Figs. 3(a) and 3(c) the following.

(i) For the narrower InAs layer, the superlattice CBM tends to the CBM of the bulk substrate: This is because the thicker the GaSb layers, the lower the overlap of the wave functions of electron levels in adjacent InAs wells, reducing the redshift of the CBM due to the level repulsion between the electron levels. Also, the thinner the InAs layer, the higher the confinement effects on the electron levels. Both effects contribute to the upshift of the superlattice CBM.

(ii) For increasing InAs thickness, a redshift of the superlattice CBM is observed: The increase in the well width pushes down the superlattice CBM, due to a reduction of the confinement effects on the electron levels in the InAs wells.

(iii) For increasing number of GaSb layers, the VBM tends to the VBM of the substrate: The hole level increases its degree of localization in the barrier region and pins at the top of the valence band.

The differences in the relative variation between the superlattice's CBM and VBM levels as a function of both InAs and GaSb thicknesses reflect the differences of the electron and hole effective masses, which are larger for the holes.

B. Band gaps

Figure 3(e) shows the band gaps, resulting from the difference between the CBM and VBM eigenvalues, as a function of the GaSb barrier thickness, for each different InAs thickness. The trends in the band gap can be analyzed into two regions.

(1) Interacting QW's: thin GaSb layers

In this regime [Fig. 3(e)], the band gap presents a nonmonotonic behavior as a function of the InAs thickness. Two regions can be recognized.

(i) *Interacting holes: Thin InAs layers*. There is a blueshift of the gap for increasing number of GaSb layers. As shown in Fig. 3(c), the VBM variation with the number of GaSb

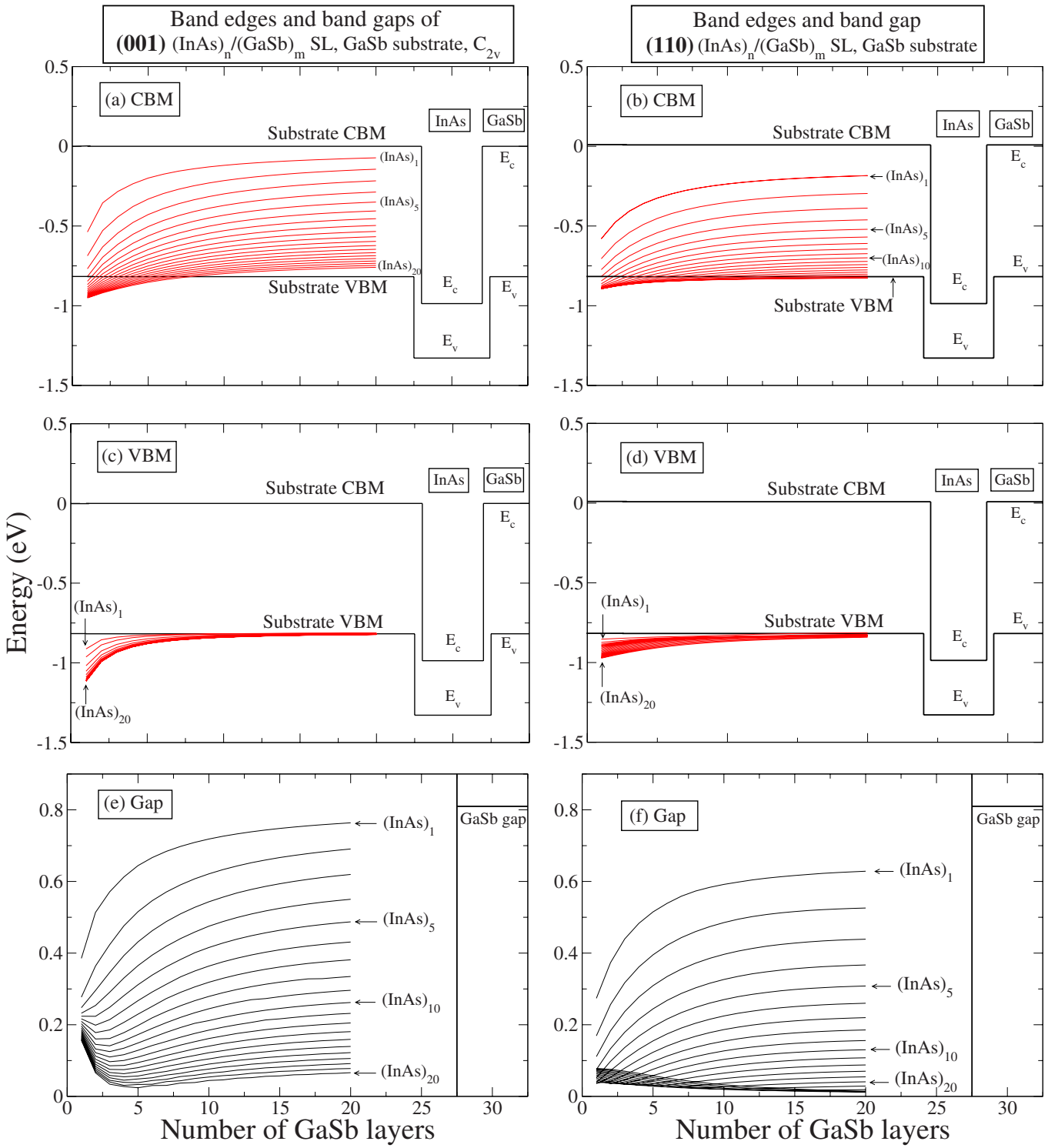

FIG. 3. (Color online) The CBM, VBM, and band gaps for the C_{2v} (001), left column, and (110), right column, $(InAs)_n/(GaSb)_m$ superlattices, on a GaSb substrate, as a function of the GaSb barrier width.

barrier layers is smaller than the corresponding CBM variation for thin $(InAs)_n$ ($n<5$) layers. Consequently, the variation of the band gap is governed by the variation in the CBM, which increases monotonically for increasing number of GaSb layers. This blueshift has already been observed experimentally[11] and is in agreement with previous theoretical calculations.[22,24]

(ii) *Isolated holes: Thick InAs layers*. In this case the gap shows a decreasing behavior for thin $(GaSb)_m$ layers ($m<4$), reaches a minimum value (not closing the gap) around $m=3-6$, and starts to increase again when the number of GaSb layers increase ($m>6$). The minimum value of the band gap for each of the $(InAs)_n$ ($n>5$) layers occurs at different thicknesses of the GaSb layer. This occurs because

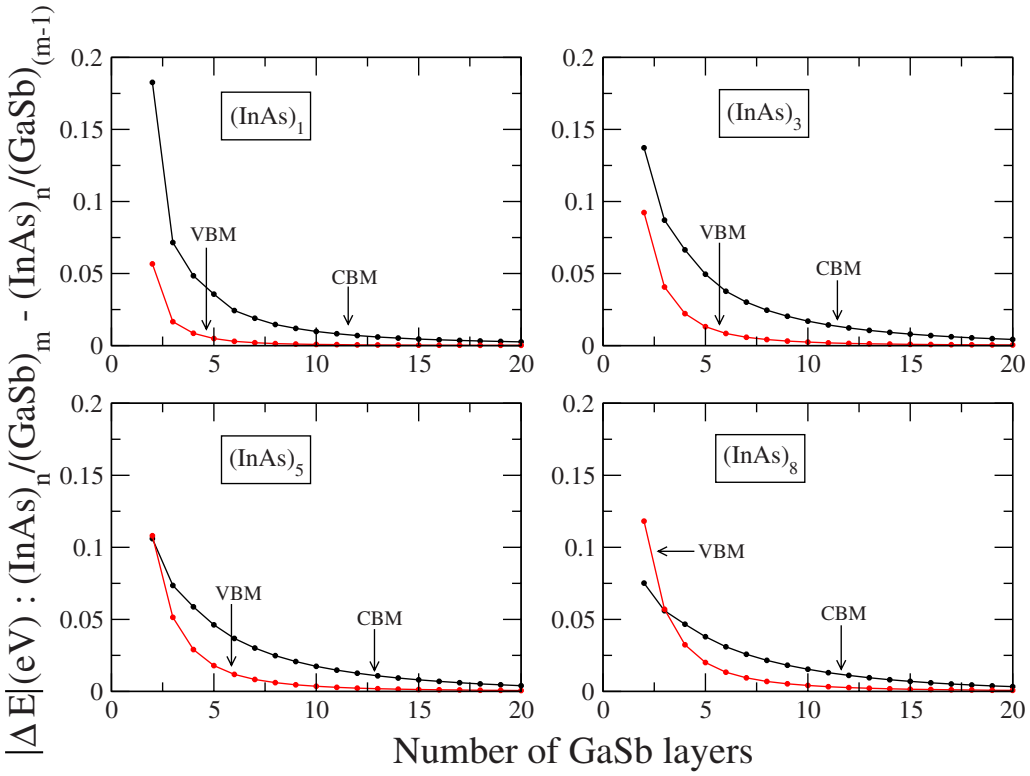

FIG. 4. (Color online) Absolute values of the change in the CBM and VBM eigenvalues when the GaSb layer width changes by one monolayer in the (001) C_{2v} $(InAs)_n/(GaSb)_m$ superlattice on a GaSb substrate, for four different InAs well widths.

the increasing thickness of the InAs wells reduces the interaction between hole levels in neighboring barriers. For narrow GaSb layers, the confinement effect on the hole levels is larger. When the number of GaSb layers increases, the confinement effect reduces its intensity and the hole levels show an upshift. This VBM upshift is larger than the CBM upshift for the same variation of the barrier thickness, which leads to a reduction of the gap value.

(2) *Toward an isolated QW regime: Thick GaSb layers*

Figure 3(e) shows the following.

(i) Blueshift of the band gap for increasing GaSb layers. The hole level is practically pinned at the energy of the substrate VBM, since the barrier widths are wide enough. The variation of the gap then follows the CBM variation, and the gap increases with increasing number of GaSb layers, due to the reduction of the electron level repulsion.

(ii) Redshift of the band gap for increasing InAs layers. The reduction of the confinement effect on the electron levels pushes down the superlattice CBM, reducing the band gap value.

The absolute value of the changes in the CBM and VBM energies as a function of the number of GaSb layers is shown in Fig. 4, for four different InAs thicknesses. It can be seen that for thin $(InAs)_n$ layers ($n<5$) the CBM variations are larger than the VBM variations for all values m of the $(GaSb)_m$ layers. For $(InAs)_n$ layers with $n>5$ and thin GaSb layers, on the other hand, the VBM variations are larger than those for the CBM. According to the trends shown in Figs. 3(a) and 3(c), the variations in the CBM and the VBM with increasing number of GaSb layers tend to increase and decrease the band gap, respectively. This illustrates the fact that the nonmonotonic behavior of the band gap for narrow GaSb layers and thick InAs layers is due to the relative intensities of the confinement effects and the repulsion energy on the hole and electron levels.

IV. DIFFERENT SUBSTRATES: GaSb vs InAs

The band gaps and band edges for the $(InAs)_n/(GaSb)_m$ superlattices on an InAs substrate are shown in Fig. 5. For comparison purposes, the results for the band gaps of these superlattices on a GaSb substrate are also shown in Fig. 5(c).

The general behavior of the variation in the CBM and VBM energies on an InAs substrate, as a function of the GaSb number of layers, is very similar to those observed in the case of a GaSb substrate. However, in this case, the substrate's CBM and VBM are those from the unstrained InAs bulk. The band edges for the strained GaSb bulk, epitaxially grown on an InAs substrate, are shown in Figs. 5(a) and 5(b). Some general trends can be observed. Only features that are not coincident with those for a GaSb substrate will be stressed.

A. Band edges

Figures 5(a) and 5(b) show the following.

(i) For thin InAs and thick GaSb layers, the superlattice CBM tends to the CBM of the strained GaSb bulk: As the thickness of GaSb layer in the superlattice turns larger, the superlattice CBM will show greater contributions from the

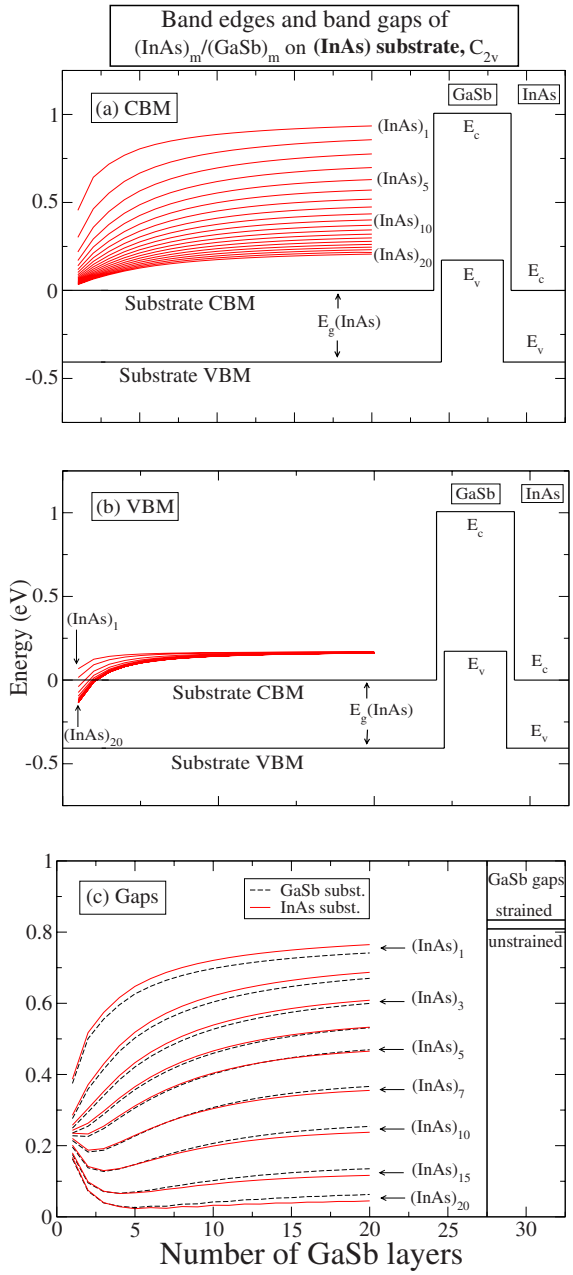

FIG. 5. (Color online) The variation of the (a) CBM, (b) VBM, and (c) band gaps for the (001) $(InAs)_n/(GaSb)_m$ superlattices, on an InAs substrate, with C_{2v} symmetry, as a function of the GaSb barrier width.

GaSb layers, tending to the CBM of the pure strained GaSb bulk material.

(ii) For thick InAs and thin GaSb layers, the superlattice CBM is lower in energy than the VBM of the strained GaSb bulk: This occurs because of the level repulsion between the electron levels in adjacent wells that shifts down the CBM energy. Also, the VBM of the GaSb strained bulk, on an InAs substrate, increases in energy (by 36 meV) relatively to the VBM of the freestanding GaSb bulk. These two factors contribute to the superlattice CBM being lower in energy than the VBM of the strained GaSb bulk.

(iii) For thick GaSb layers, the superlattice VBM tends to the VBM of the strained GaSb bulk: Since the effective mass of the hole levels is relatively higher than the electron effective mass (which reduces the changes in the hole level energy due to confinement effects), and since the hole levels are mainly localized in the GaSb barrier region, the increase in the number of GaSb layers leads to the pinning of the superlattice VBM energy at the VBM level of the strained GaSb bulk.

The characteristic behavior of the superlattice's CBM and VBM for these short-period $(InAs)_n/(GaSb)_m$ superlattices on InAs and GaSb substrates shows similarities but the eigenvalues are certainly not identical. The differences in the superlattice's CBM and VBM energies, due to the difference in the in-plane lattice constants of the InAs and GaSb substrates, are reflected in the band gaps of the superlattices.

B. Band gaps

The constraints imposed by the different substrates act differently on the InAs and GaSb layers of the superlattices. In the case of a GaSb substrate, a tensile strain appears in the InAs layers, while the GaSb layers are strain-free. As a consequence of this tensile strain on the InAs layers, an average increase of the In-As bonds will occur. On the other hand, the InAs substrate imposes a compressive strain on the GaSb layers, while keeping the InAs layers strain-free. This will lead to a reduction in the Ga-Sb average bond distances. The consequences of these effects on the band gaps are seen in Fig. 5(c), where the variation of the band gaps of the superlattices as a function of the number of GaSb layers on both substrates is shown. Two distinct behaviors can be seen.

(1) Delocalized electron levels: Thin $(InAs)_n$ *layers,* $n \leqslant 5$

(i) The band gaps of the superlattices on a GaSb substrate are lower in energy than those on an InAs substrate: This occurs because the relatively small content of InAs layers in the superlattices makes the CBM level delocalized along the superlattice. In this case, the influence of the strain fields on the band gaps will be mainly determined by the behavior of the GaSb layers on strain, since both electron and hole levels have larger contributions at the barrier regions. Since the band gap of the strained GaSb bulk on an InAs substrate is larger than the band gap of the freestanding GaSb bulk, as shown in the column at the right side of Fig. 5(c), the band gaps of the superlattices on InAs substrates will be larger.

(2) Increasing confinement of the electron level: Thick $(InAs)_n$ *layers,* $n > 5$

(i) The band gaps of the superlattices on a GaSb substrate are higher in energy than those on an InAs substrate: This is because the increase in the relative number of InAs layers in the superlattices increases the degree of localization of the electron level on the InAs well region. The electron and hole levels will be spatially separated in the well and barrier regions of the superlattices, respectively. In the limit case of both InAs and GaSb being thick, the superlattice CBM (VBM) energy will approach the CBM (VBM) of the InAs (GaSb) bulk material. The VBM level of the GaSb bulk is higher in energy in the InAs substrate (−4.98 eV, with respect to vacuum) than in the freestanding case (−5.02 eV). The same energetic ordering is observed for the CBM level

of the InAs bulk, being higher in energy on the InAs (−5.16 eV) than on the GaSb (−5.20 eV) substrates. By calculating the difference between the CBM level in the InAs bulk and the VBM level in the GaSb bulk materials on both substrates, the band gap in the limit of thick InAs and GaSb layers can be determined. These band gaps are 0.18 and 0.14 eV (difference of 0.04 eV) for GaSb and InAs substrates, respectively. The same difference calculated for the $(InAs)_{20}/(GaSb)_{20}$ superlattice gives 0.018 eV, with the GaSb band gap being higher in energy. Hence, as both InAs and GaSb layers in the superlattices turn thicker, larger will be the difference between the band gaps on InAs and GaSb substrates, with the last case presenting larger band gap values.

As seen from Fig. 5(c), the change in the energetic ordering between the band gaps for $(InAs)_n/(GaSb)_m$ superlattices on the InAs and GaSb substrates occurs at different GaSb thicknesses, for each number of InAs layers. The crossing point changes from $m \simeq 14$ at $n=5$ to $m \simeq 4$ to $n=20$. For $n<5$, the band gaps of the superlattices on an InAs substrate are always higher than those for a GaSb substrate.

V. DIFFERENT POINT GROUP SYMMETRIES: C_{2v} vs D_{2d}

The (001) superlattices with C_{2v} symmetry all have integer numbers of InAs and GaSb monolayers [each monolayer consisting of one cation plus one anion atomic layers in the (001) direction]. In this way, the atomic bonds at adjacent interfaces will alter from In-Sb to Ga-As. On the other hand, $(InAs)_n/(GaSb)_m$(001) superlattices with D_{2d} symmetry require that both the InAs and GaSb layers have a half-integer number of monolayers to fulfill the symmetry constraints. For example, a typical D_{2d} (001) superlattice with In-Sb bonds at the interfaces will have the following sequence of atomic planes:

$$\cdots \text{–In-As-In-As-In-Sb-Ga-Sb-Ga-Sb-In-As-In-As-In}\cdots$$

where an odd number of atomic planes is required in each InAs or GaSb layers. A similar pattern would be required for (001) superlattices with D_{2d} point group symmetry and Ga-As bonds at the interfaces.

A. Band edges

Figures 6(a)–6(f) compare the calculated CBM and VBM eigenvalues for $(InAs)_n/(GaSb)_m$ superlattices grown in the (001) direction with different point group symmetries, D_{2d} and C_{2v}. For the superlattices with D_{2d} symmetry, the bonds at the interfaces are exclusively either In-Sb (D_{2d}/In-Sb) or Ga-As (D_{2d}/Ga-As). A comparison of these figures shows the following.

(i) The D_{2d} superlattice, with In-Sb bonds at the interfaces, shows a reduced spread in energy of the CBM levels as a function of the InAs thickness, as compared to the C_{2v} and D_{2d}/Ga-As cases.

(ii) For thin GaSb layers, the superlattice's CBM and VBM energies are lower in energy for the D_{2d}/Ga-As than for the D_{2d}/In-Sb superlattices.

(iii) For $(InAs)_n$, $n \leqslant 3$, the VBM of the D_{2d}/In-Sb superlattices shows a blueshift for decreasing number of GaSb layers.

(iv) For $(InAs)_n$, $n>3$, the VBM of the D_{2d}/In-Sb superlattices presents the lowest variation as a function of both InAs and GaSb thicknesses.

A conclusion from the above set of observations is that the presence of In-Sb bonds at each interface in the D_{2d}/In-Sb superlattices pins the center of gravity of the CBM and VBM levels, reducing the influence of the variation of the well and barrier widths on the band edge energies due to confinement and level repulsion effects. For the D_{2d}/Ga-As superlattices, the Ga-As bonds at the interfaces increase the electrostatic potential acting on the superlattice and push down the single-particle energy levels.

B. Band gaps

The band gaps for the D_{2d}/In-Sb, D_{2d}/Ga-As, and C_{2v} $(InAs)_n/(GaSb)_m$ superlattices, on a GaSb substrate, are shown in Figs. 6(g)–6(i). Two regions can be recognized.

(1) Delocalized electron level: Thin $(InAs)_n$ *layers*, $n \leqslant 5$.

(i) All superlattices present a blueshift for increasing number of GaSb layers: The increasing rate of the band gap value for thin GaSb layers is greater for the C_{2v} and D_{2d}/In-Sb superlattices.

(ii) For thin $(GaSb)_m$ layers ($m<5$), the band gaps of the superlattices show the following order: D_{2d}/Ga-As $> C_{2v}$ $> D_{2d}$/In-Sb. The exception being the case of $(InAs)_1$, for which the C_{2v} superlattice shows the highest band gap.

(2) Increasing confinement of the electron level: Thick $(InAs)_n$ *layers*, $n>5$.

(i) For $(InAs)_n$, $6<n<12$, the band gaps of D_{2d}/Ga-As superlattices, Fig. 6(h), show a nonmonotonic behavior of the band gap, similar to that for the C_{2v} case, already discussed, although less pronounced.

(ii) For $(InAs)_n$, $n>12$, the band gaps for the D_{2d}/Ga-As superlattices show a redshift, which tend to a saturation, for increasing number of GaSb layers.

(iii) For thin $(GaSb)_m$ layers, $m<9$, an anticrossing between the electron and hole levels leads to a blueshift of the D_{2d}/In-Sb superlattice gap. The charge densities for the CBM and VBM levels in Fig. 7 illustrate this point. As the GaSb layers turn wider, the band gap shows a redshift, presenting a minimum value that approaches but does not touch the zero gap value. Further increase in the GaSb number of layers leads to a blueshift of the band gap, with oscillations. The oscillations in the gap value are due to an even and/or odd oscillation in the coupling intensities between the states pinned by the In-Sb interfaces.

From these observations it can be seen that the presence of In-Sb bonds at the interfaces reduces the band gap of the superlattices. This influence is more pronounced for superlattices with a small number of GaSb layers, where the variation of the VBM eigenvalues is significant, with the superlattice VBM eigenvalues increasing in energy as greater the number of In-Sb bonds at the interfaces. Actually, for the D_{2d}/In-Sb superlattice, it leads to an anticrossing between

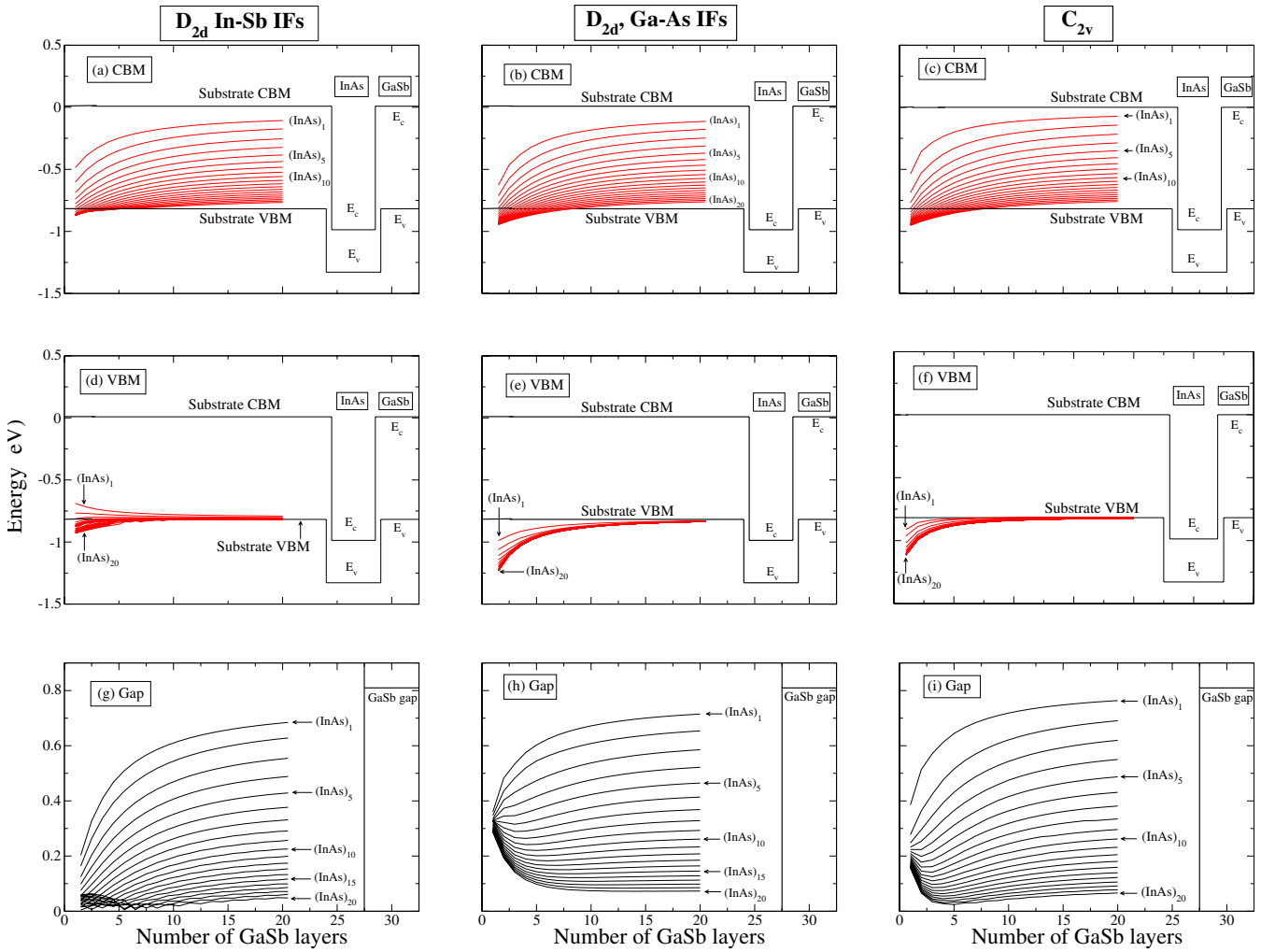

FIG. 6. (Color online) The conduction band maximum eigenvalues for the (001) $(InAs)_n/(GaSb)_m$ superlattices and D_{2d} point group symmetry with (a) In-Sb and (b) Ga-As bonds at the interfaces, as well as for the (c) C_{2v} point group symmetry superlattices. The valence band minimum for the superlattices with D_{2d} point group symmetry and (d) In-Sb and (e) Ga-As bonds at the interfaces, as well as for the (f) C_{2v} point group symmetry superlattices. The band gaps for the D_{2d} superlattices and (g) In-Sb and (h) Ga-As bonds at the interfaces, as well as the (i) C_{2v} point group symmetry superlattices.

the electron and hole levels, the gap not being zero due to the underlying symmetry of the superlattice.

VI. DIFFERENT LAYER ORIENTATION: (001) vs (110)

The characteristic feature of the (110) superlattices is that, differently from the cases discussed so far, their interfaces are nonpolar, presenting both cations and anions in equal proportion at each abrupt interface. All interfaces will show both In-Sb and Ga-As bonds. The interfaces at each side of a given layer can be symmetry related through a mirror plane reflection or by the inversion symmetry operator. When the InAs and GaSb layers are composed by an odd number of atomic planes, the mirror symmetry is fulfilled. On the other hand, for an even number of atomic planes in both InAs and GaSb layers, the inversion symmetry is observed.

The CBM and VBM levels for the (110) $(InAs)_n/(GaSb)_m$ superlattices with mirror symmetry, as a function of the number of GaSb layers, are shown on Figs. 3(b) and 3(d), respectively, for each $(InAs)_n$ well width ($n=1,20$). The CBM and VBM levels for the (110) $(InAs)_n/(GaSb)_m$ superlattices with inversion symmetry are very similar to those shown in Figs. 3(b) and 3(d) and are not explicitly shown here. However, when differences between the two types of (110) superlattices occur, they are presented in the following discussion. An analysis of these figures reveals the following aspects.

A. Band edges

From Figs. 3(b) and 3(d), the following is seen.

(i) The CBM eigenvalues for the (110) superlattices with mirror symmetry are always lower in energy as compared to those with inversion symmetry: The symmetric combination of the wave functions in adjacent interfaces for the superlattices with mirror symmetry intensifies the effect of level repulsion on the electron levels, leading to lower energies for the CBM levels in the (110) superlattices with mirror symmetry.

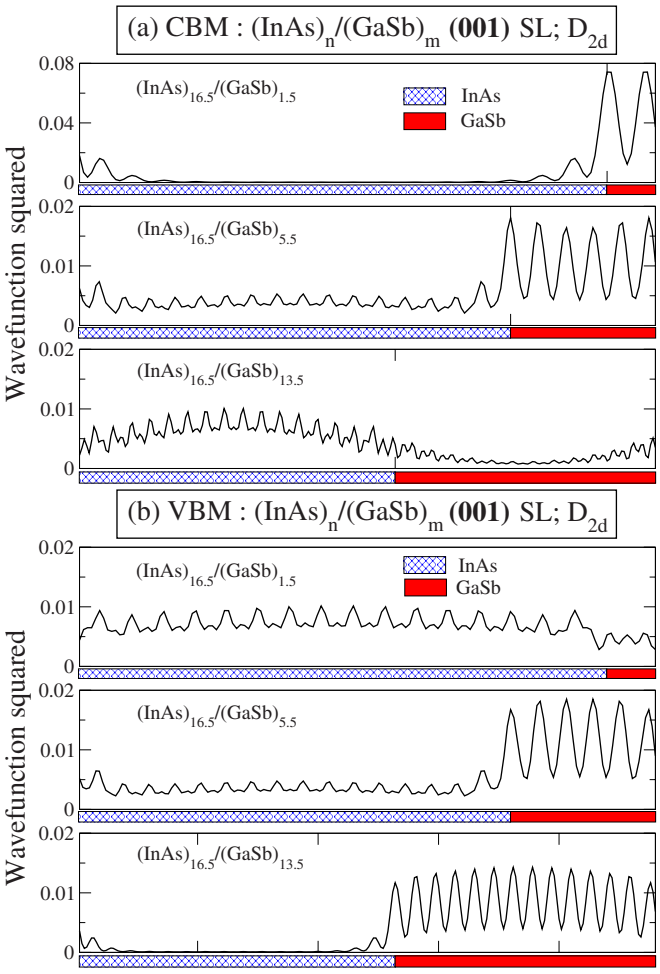

FIG. 7. (Color online) Squared wave functions of the (a) CBM and (b) VBM levels along the growing direction of the (001) $(InAs)_n/(GaSb)_m$ superlattices, with D_{2d} point group symmetry, on a GaSb substrate. The crossed and filled regions represent the InAs and GaSb layers. The numbers of InAs and GaSb monolayers are indicated inside the figures.

(ii) The CBM levels in the (110) superlattices with both mirror and inversion symmetries, for the thicker InAs layers, remain below the substrate's VBM level for all range of GaSb layers.

(iii) For thin GaSb layers, the VBM levels of both mirror and inversion symmetry (110) superlattices present a small dispersion with the variation of number of InAs and GaSb layers: The level repulsion due to the interaction of hole levels in adjacent barriers, for thin GaSb layers, is largely reduced as compared to the same effect for the C_{2v} point group symmetry (001) $(InAs)_n/(GaSb)_m$ superlattices (Sec. III A). This is related to the influence of the In-Sb bonds at each interface, which pin the center of gravity of the band edges in the (001) superlattices.

(iv) In both mirror and inversion symmetry (110) superlattices there is an anticrossing between the light- and heavy-hole levels for one and two InAs layers, as a function of the GaSb thickness. A representative case of this anticrossing is shown in Fig. 8, for the mirror symmetry (110) superlattice.

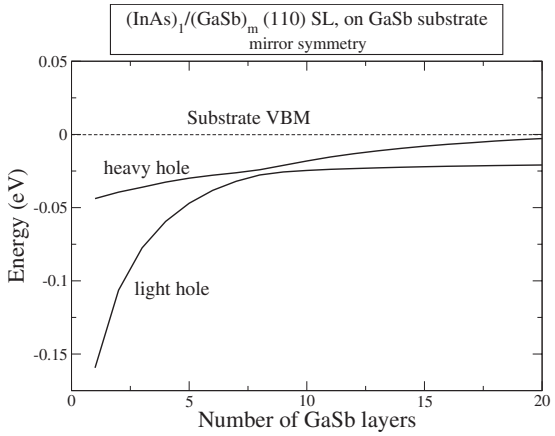

FIG. 8. Anticrossing between light and heavy holes for the $(InAs)_1/(GaSb)_m$ $(m=1,20)$ (001) superlattices.

B. Band gaps

The band gap behavior of the (110) $(InAs)_n/(GaSb)_m$ superlattices is shown in Fig. 3(f), as a function of the number of GaSb layers, for each value of the $(InAs)_n$ well width ($n=1,20$). The main observations are the following.

(i) The band gaps of the mirror symmetry (110) superlattices are always lower than those for the inversion symmetry (110) superlattices.

(ii) For thick $(InAs)_n$ layers, $n>9$, and thin GaSb layers, the band gap shows a blueshift with increasing number of InAs layers and a redshift with increasing number of GaSb layers. This is due to an anticrossing between the electron and hole levels of the superlattices. This anticrossing can be seen from Figs. 9(a) and 9(b), where it is shown that for thin GaSb layers the CBM (VBM) level has greater concentration on the GaSb (InAs) layers, whereas for thick GaSb layers the CBM (VBM) level has greater concentration on the InAs (GaSb) layers of the superlattice.

(iii) For thick $(InAs)_n$ layers, $n>9$, and thick (GaSb) layers, the band gaps show a small blueshift with increasing number of GaSb layers and a redshift with increasing number of InAs layers.

VII. ORDERED SUPERLATTICES vs RANDOM ALLOYS

In this section we present the comparison among some of the ordered superlattices studied in previous sections with random alloys, for different In compositions, on GaSb substrates. In order to assure the lattice matching condition of the random alloys to a GaSb substrate, the (x,y) composition of a generic $In_xGa_{1-x}As_ySb_{1-y}$ alloy should obey the following algebraic equation:[1]

$$y = 0.001 + 0.648x + 0.239x^2. \quad (6)$$

Once the In composition is given, the composition of all other elements in the alloy is determined. It should be stressed that, due to the constraint imposed by Eq. (6), the random alloy compounds with 0.0% and 100% In compositions do not possess corresponding As compositions of 0.0%

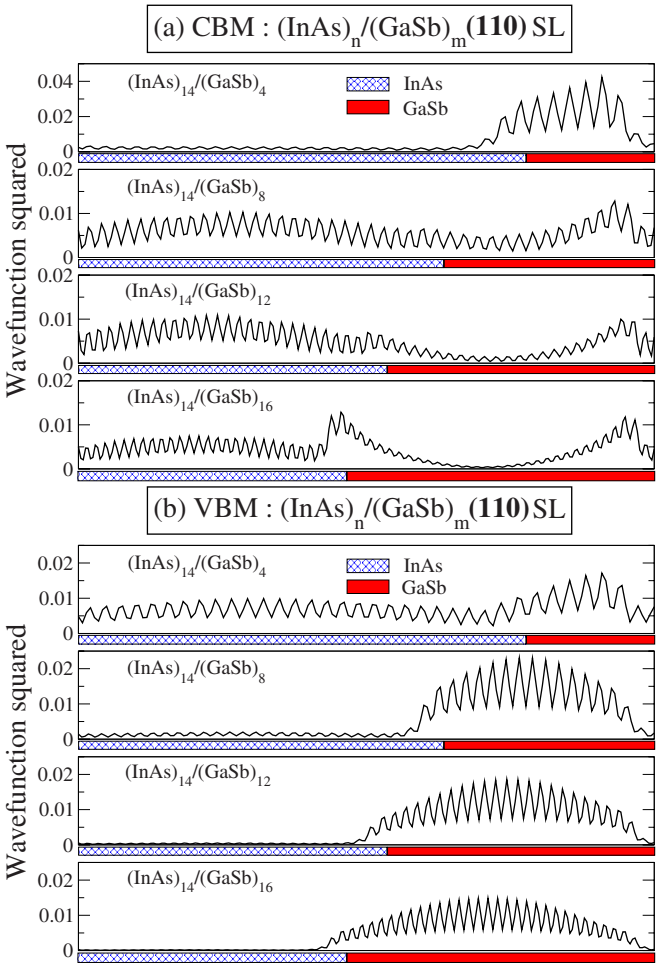

FIG. 9. (Color online) Squared wave functions of the (a) CBM and (b) VBM levels along the growing direction of the (110) $(InAs)_n/(GaSb)_m$ superlattices, on a GaSb substrate. The crossed and filled regions represent the InAs and GaSb layers. The numbers of InAs and GaSb monolayers are indicated inside the figures.

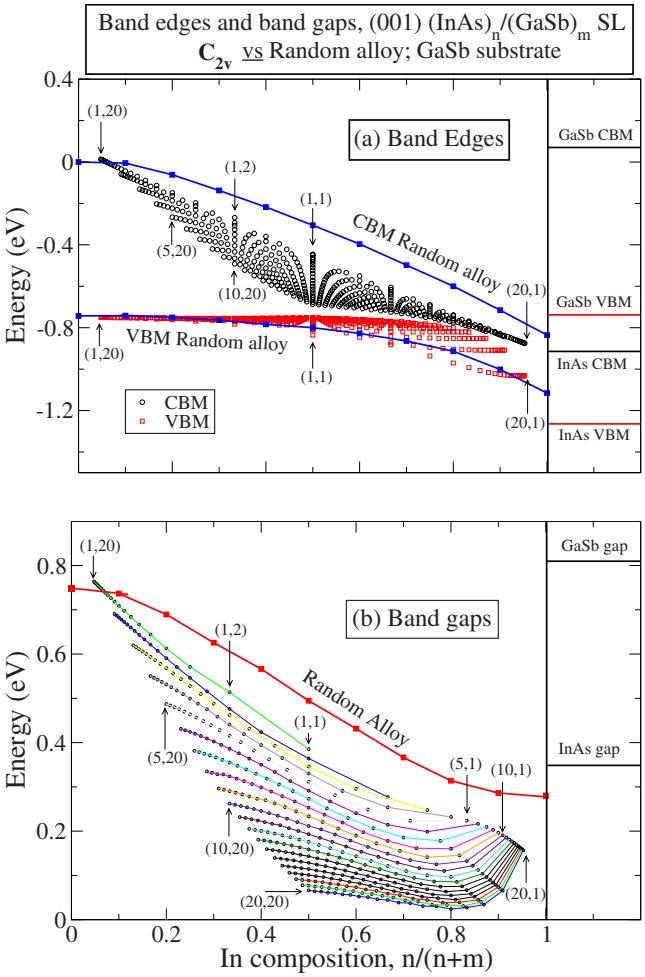

FIG. 10. (Color online) The (a) band edges and (b) band gaps for the (001) $(InAs)_n/(GaSb)_m$ $(n,m=1,20)$, C_{2v} superlattices and random alloys, lattice matched to a GaSb substrate, for different In compositions.

and 100%, as is the case for the ordered superlattices, where the In/As composition ratio is 1.

In general, the higher band gaps in random alloys, as compared to ordered superlattices, can be traced to the different folding of k points in the irreducible Brillouin zone. The random alloys will have many folded k points, with a weak repulsion among the folded levels. However, the ordered superlattices will have comparatively few folded k points and a strong repulsion between the folded levels, which tends to lower the CBM and raise the VBM levels, thus leading to reduced band gaps. Also, the numbers of In-As and Ga-Sb (In-Sb and Ga-As) bonds in the superlattices are larger (smaller) than those in the random alloys. For the superlattices, the In-Sb and Ga-As bonds appear only at the interfaces, while for the random alloys they are spread over the whole sample. This affects the behavior of the band edges and band gaps according to the results shown in Sec. V, where we showed that an excess of In-Sb bonds at the interfaces leads to smaller gaps, due to the corresponding changes in the band edge energies.

A. Random alloys vs (001) $(InAs)_n/(GaSb)_m$ superlattices with C_{2v} symmetry

1. Band edges

The VBM and CBM of the random alloys and those for the (001) $(InAs)_n/(GaSb)_m$ superlattices, with C_{2v} symmetry are shown in Fig. 10(a). A comparison between the values for the random alloys and the ordered superlattices allows the following observations.

(i) The CBMs of the superlattices are almost always lower in energy as compared to the random alloy values. The exception being the cases $(InAs)_1/(GaSb)_m$, $m=19,20$. As noted above, this is a consequence of the greater level repulsion in the superlattices due to the level folding. The larger differences between the CBM values of the superlattices and the random alloy appear around In composition of 50%.

(ii) The dispersion of the superlattices' CBM is reduced for In-rich compositions (thick InAs wells).

(iii) For In compositions lower than 30% (thick GaSb barriers), the VBMs of the superlattices and the random alloy practically coincide in energy, indicating the localization of the hole levels in the superlattices.

(iv) For In compositions higher than 30%, the VBM for the majority of the superlattices is higher in energy than the VBM of the corresponding random alloy. However, the VBM of the $(InAs)_n/(GaSb)_1$ $(1 \leqslant n < 12)$ superlattices is seen to be lower in energy than the VBM of the random alloy for In compositions from 0.5 to 0.9, indicating that the confinement effects of the hole levels in the GaSb barriers can even surpass the effects due to the natural localization of wave functions in random alloys.

(v) The fact that the CBM and VBM levels of the random alloys do not match those of the InAs bulk at the 100% limit of In composition is that, as pointed above, the lattice matching condition given by Eq. (6) imposes a nonzero Sb content as well as As composition different from 100%.

2. Band gaps

The band gaps for the random alloys and for the (001) (InAs)/(GaSb) superlattices, with C_{2v} point group symmetry, are shown in Fig. 10(b). A comparison between the band gaps for the random alloys and the ordered superlattices shows the following.

(i) The band gaps of the (001) C_{2v} superlattices are lower than those of the random alloys for almost all In compositions. The exceptions being the $(InAs)_1/(GaSb)_m$, $m=19,20$ superlattices, which show slightly higher band gaps, as compared to the random alloys;

(ii) The random alloy band gaps show a decreasing behavior for increasing In composition, while for the (001) C_{2v} superlattices, the decreasing behavior is observed for In composition lower than 80%. For higher In contents, the $(InAs)_n/(GaSb)_m$ with $n \geqslant 12$ superlattices show band gaps that increase for increasing In composition, with a rate that is greater for larger n/m ratios.

B. Random alloys vs (001) $(InAs)_n/(GaSb)_m$ superlattices with D_{2d}/In-Sb symmetry

1. Band edges

The CBM and VBM energy values and the band gaps for the (001) $(InAs)_n/(GaSb)_m$ superlattices, with D_{2d} symmetry and In-Sb bonds at the interface, and for the random alloys are shown in Figs. 11(a) and 11(b), respectively. As far as the band edges are concerned, we can say the following.

(i) The CBMs for the superlattices are lower than those for the random alloys, approaching the random values for In-rich and In-poor extrema. The largest differences are observed for In compositions around 30%–40%.

(ii) The VBMs for the superlattices show an almost constant behavior for In composition lower than 70%. A small decrease of the VBM for the In-rich superlattices is observed.

(iii) For the $(InAs)_1/(GaSb)_m$ superlattices, the VBM shows an increasing behavior, for increasing In composition. The VBM of the $(InAs)_1/(GaSb)_1$ is barely seen among the CBM values at the 50% composition.

2. Band gaps

The comparison of the band gaps for the (001) (InAs)/(GaSb) superlattices, with D_{2d} symmetry and In-Sb bonds at the interfaces with the random alloys, both lattice matched with a GaSb substrate, as shown in Fig. 11(b), allows us to make the following observations.

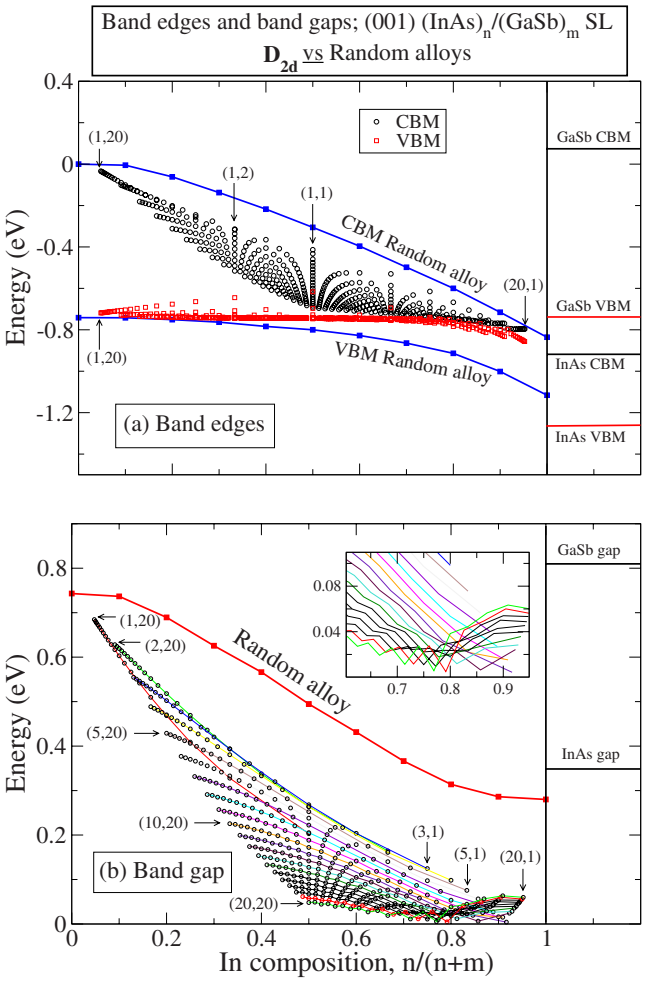

FIG. 11. (Color online) The (a) band edges and (b) band gaps for the (001) $(InAs)_n/(GaSb)_m$ $(n,m=1,20)$, D_{2d} superlattices and random alloys, lattice matched to a GaSb substrate, for different In compositions.

(i) The band gaps for the (001) D_{2d}/In-Sb superlattices are lower than for the random alloys. The difference increases with increasing In composition.

(ii) The (001) D_{2d}/In-Sb band gaps for In composition $\geqslant$80% are all $\leqslant$0.1 eV, around 0.2 eV lower than the band gaps of the random alloys with the same In composition.

(iii) The (001) D_{2d}/In-Sb band gaps show a blueshift for In composition greater than 80%, which increase in intensity as larger the n/m ratio in the $(InAs)_n/(GaSb)_m$ superlattices.

C. Random alloys vs (110) $(InAs)_n/(GaSb)_m$ superlattices

1. Band edges

The band edges for the (110) superlattices with mirror symmetry and for the random alloys, lattice matched to GaSb substrate, as a function of the In composition, are shown in Fig. 12(a).

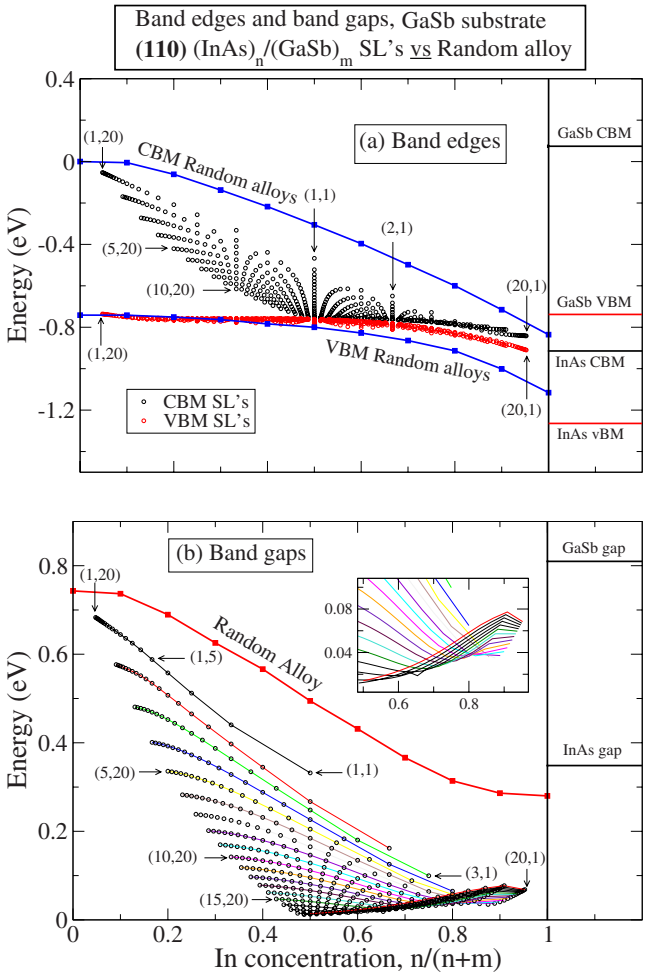

FIG. 12. (Color online) The (a) band edges and (b) band gaps for the (110) $(InAs)_n/(GaSb)_m$ $(n,m=1,20)$ superlattices and random alloys, lattice matched to a GaSb substrate, for different In compositions.

(i) The CBMs for the (110) superlattices are lower than those for the random alloys, for all In compositions. The difference being higher for In compositions between 30% and 70%.

(ii) The dispersion of the CBM values of the (110) superlattices is smaller in the In-rich limit than in the In-poor limit.

(iii) The VBMs of the superlattices are almost identical to the VBM of the random alloys for In composition $\leqslant 30\%$. For higher In compositions, the VBMs of the superlattices are higher in energy than the VBM of the random alloy, with the difference increasing for increasing In composition. There is almost no dispersion of the superlattice VBM values for all In compositions.

2. Band gaps

Considering the comparison between the band gaps of the (110) superlattices and the random alloys, shown in Fig. 12(b) as a function of the In composition, the following observations can be made.

(i) The band gaps of the (110) superlattices are lower than those for the random alloys with the same In composition.

(ii) The band gaps of the $(InAs)_n/(GaSb)_m$, with $n \geqslant 8$, present a blueshift for a range of m values. For example, for $n=20$, 19, and 18, the blueshift occurs for all the m values, while for $n=17$, the band gap decreases for $9<m\leqslant 20$ and then increases for $m<9$, and for $n=10$, the gap decreases for $3<m\leqslant 20$ and increases for $m<3$.

The above classification of the band edges and band gaps of different (InAs)/(GaSb) superlattices as a function of the In composition allows one to select, among the various possible superlattice configurations, the ones who present a desirable gap. Also, given a desired gap, to select the thicknesses of the (InAs) and (GaSb) layers that satisfy the established gap criterion.

VIII. EFFECTS OF INTERFACIAL INTERMIXING ON THE BAND GAPS

The band gap results presented in the previous sections are for abrupt interfaces and do not take into account atomic interdiffusion that occur in the layers close to the interfaces.[28] The atomic interdiffusion leads to changes in the observed band gaps. This fact is supported by the observation of a 30–40 meV band gap variation by changing the growing temperatures of similar superlattices grown in otherwise identical conditions.[61]

We have calculated segregation profiles by using a kinetic model for molecular beam epitaxy growth,[62] which was extended to treat both cation and anion interdiffusion processes.[23] In this kinetic model, a layer by layer growth mode is assumed. The rate of change of the surface concentration of an atomic species labeled A (in a sublattice with A and B atoms) at a certain time t, $x_A^s(t)$, is given by[23]

$$\frac{dx_A^s(t)}{dt} = \Phi_A + P_1 x_A^b(t) x_B^s(t) + P_2 x_A^s(t) x_B^b(t), \qquad (7)$$

where Φ_A is the deposition rate of atoms A (in monolayers/s) and P_i represents the probability of an atomic exchange between the bulk (subsurface layer) and the surface regions, where the concentrations of A atoms, for example, are given by x_A^b and x_A^s, respectively.[63] It is important to note that $\mathbf{k}\cdot\mathbf{p}$ calculations in effect fit their theory of chemically *abrupt* interfaces to experiments which are clearly nonabrupt, thus missing a genuine physical effect.

Tables I and II show a comparison between the results obtained for the $(InAs)_n/(GaSb)_m$ superlattices both with abrupt and interdiffused interfaces and the available experimental band gap values as well as to previous $\mathbf{k}\cdot\mathbf{p}$ calculations.[24] The superlattices whose calculated and experimental band gaps are compared are identified by the period and/or number of monolayers, as well as the type of atomic bonds at the interfaces. The results in Tables I and II show that the calculated band gap values for the abrupt interfaces are lower than the experimental ones, with the difference diminishing as the thicknesses of the InAs and GaSb layers increase. For example, the difference between the experimental band gap results and the calculated abrupt ones is

TABLE I. Calculated (abrupt) and experimental band gaps of selected (001) D_{2d} $(InAs)_n/(GaSb)_m$ superlattices on a GaSb substrate with In-Sb bonds at the interfaces, as a function of the periods and layer thicknesses. The experimental values are taken from Refs. 5, 8, and 24. The values for the InAs/GaSb thicknesses are the measured values.

	Expt.		Calc. (abrupt)	
InAs/GaSb (Å)	Period (Å)	Band gap (meV)	Period (Å)	Band gap (meV)
20.5/18	40.4	254.5	39.8	237.9
20.5/21	44.1	279	42.8	260.9
20.5/24	46.2	293	45.8	280.3
20.5/27	49.3	299	48.9	296.7
26/15	46.3	191.6	45.7	168.5
26/18	47.7	205.3	48.8	189.0
26/21	50.8	210.5	51.8	205.3
26/24	54.2	217.9	54.9	220.6
26/27	56.5	236.6	57.9	232.2
16/24		370.5	42.8	326.5
19/24		324.3	45.8	280.3
23.5/24		265.6	48.8	240.5

23.1 meV for the $(InAs)_{26}/(GaSb)_{15}$ and 4.4 meV for $(InAs)_{26}/(GaSb)_{27}$ superlattices. Since the atomic segregation affects mainly the layers near the interfaces, the relative number of layers affected by the atomic segregation, and hence the influence of the segregation profiles will be greater for short-period superlattices.

We have applied the kinetic model for atomic segregation for two $(InAs)_n/(GaSb)_m$ selected superlattices, namely, $(InAs)_6/(GaSb)_6$ and $(InAs)_6/(GaSb)_{12}$. The results are shown in Table II. The calculated band gaps increase, as compared to the abrupt interfaces, leading to a good agreement with the experimental values. They confirm the tendency shown in previous atomistic pseudopotential calculations[17,22,23,29] of the segregation to increase the band gap values, as well as the bigger impact of the segregation on the band gaps of superlattices with smaller periods. Note that $\mathbf{k}\cdot\mathbf{p}$ calculations lack the physics of chemical segregation and show gaps with nonsystematic trends: calculated gaps are sometimes larger and sometimes smaller than the experimental values.

IX. CONCLUSIONS

Plane-wave empirical pseudopotential calculations for the short-period $(InAs)_n/(GaSb)_m$ superlattices show that the band gaps and band edges depend on different factors as atomic bonds at the interfaces, point group symmetry of the superlattices, layer orientation, and substrate. For the (001) C_{2v} superlattices on a GaSb substrate, the band gaps show different behaviors depending on the relative width of the

TABLE II. Calculated and experimental band gaps of selected (001) C_{2v} $(InAs)_n/(GaSb)_m$ superlattices on a GaSb substrate, as a function of the periods and the numbers of (InAs)/(GaSb) monolayers. The calculated gaps are shown for interfaces with abrupt and segregated (taken at 380 °C) composition profiles. The $\mathbf{k}\cdot\mathbf{p}$ values are taken from Ref. 24. The absorption spectroscopy (Abs.) and photoluminescence (PL) experimental values are taken from Refs. 10 and 11.

InAs/GaSb MLs	Band gap (meV)				
	Expt.		Calc.		
			Atomistic		$\mathbf{k}\cdot\mathbf{p}$
	Abs.	PL	Abrupt	Segregated	Abrupt
6/6	326	318	263.1	330.19	315.1
6/9	358	355	322.9		365.4
6/12	386	382	362.3	409.3	396.5
6/18	416	415	404.1		427.9
8/8	283	277	230.3		273.3
8/12	308	304	278.8		310.6
8/16	332	330	306.3		330.3

GaSb barriers and the InAs wells. For thin $(InAs)_n$ layers ($n<5$), the band gap presents a blueshift with increasing number of GaSb layers. For thick $(InAs)_n$ ($n \geqslant 6$) layers, the band gaps show a nonmonotonic behavior, as a function of the GaSb thickness. For thin GaSb layers the band gaps show a blueshift as a function of the InAs layers. As the GaSb layer thickness is progressively increased, the band gap shows a redshift, passing through a minimum value (>0) and finally a blueshift.

The band gap behavior of the (001) C_{2v} superlattices on different substrates, InAs, and GaSb, will depend on the degree of localization of the electron level (conduction band maximum). For thin InAs wells, the electron levels will be mostly delocalized along the superlattice, and the influence of the different strain fields on the band gaps will be determined mostly by the behavior of the GaSb layers on strain. The superlattices with thin InAs will present larger band gaps on InAs substrates. As the InAs wells turn thicker, the VBM and CBM levels from the superlattices follow the behavior of the corresponding levels in their parent bulk on strain, leading gradually to smaller band gaps on InAs substrate.

The band gaps of (001) D_{2d} superlattices present different behaviors depending on the type of atomic bonds at the interfaces. The superlattices with In-Sb bonds at the interfaces show reduced band gap values, as compared to the (001) C_{2v} case, due to the pinning of the band edge states by the In-Sb bonds. On the other hand, the D_{2d} superlattices with Ga-As bonds at the interfaces present larger band gaps than both C_{2v} and D_{2d}/In-Sb superlattices.

The superlattices with (110) layer orientation show a reduced variation of the band edge states as a function of both the InAs and GaSb thicknesses, as compared to the (001) C_{2v} case. The band gaps for the (110) superlattices are also smaller than the corresponding values for (001) C_{2v}. An anticrossing between the light and heavy-hole levels occurs for thin GaSb and thick InAs layers.

The comparison of the band edges and band gaps between the superlattices grown on a GaSb substrate and the random alloys lattice matched to a GaSb substrate, with the same In composition, show that the band gaps and CBM (VBM) values of the random are almost always higher (lower) than the corresponding values in the superlattices. It gives a direct quantitative indication of the influence of the superlattice's ordering and period on the band gap and band edges. Also, it allows us to compare the degree of localization of the band edge states among the superlattices and between the superlattices and the random alloys.

A comparison between the calculated band gaps for the superlattices with abrupt and interdiffused interfaces with some available experimental data shows that the atomic interdiffusion in the layers close to the interfaces tends to increase the band gap values, with greater influence on superlattices with the shortest periods.

ACKNOWLEDGMENTS

This work was funded by the U.S. Department of Energy, Office of Science, Basic Energy Sciences, Materials Science and Engineering, under Contract No. DE-AC36-99GO10337 to NREL.

*Permanent address: Departamento de Física, Universidade Federal de Santa Maria, 97105-900 Santa Maria, RS, Brazil.

[1] R. Magri, A. Zunger, and H. Kroemer, J. Appl. Phys. **98**, 043701 (2005).
[2] G. A. Sai-Halasz, L. Esaki, and W. A. Harrison, Phys. Rev. B **18**, 2812 (1978).
[3] L.-W. Wang, S.-H. Wei, T. Mattila, A. Zunger, I. Vurgaftman and J. R. Meyer, Phys. Rev. B **60**, 5590 (1999).
[4] H. J. Haugan, F. Szmulowicz, G. J. Brown, and K. Mahalingam, J. Appl. Phys. **96**, 2580 (2004).
[5] H. J. Haugan, F. Szmulowicz, G. J. Brown, and K. Mahalingam, Appl. Phys. Lett. **84**, 5410 (2004).
[6] H. J. Haugan, F. Szmulowicz, K. Mahalingam, G. J. Brown, S. R. Munshi, and B. Ullrich, Appl. Phys. Lett. **87**, 261106 (2005).
[7] H. J. Haugan, K. Mahalingam, G. J. Grown, W. C. Mitchel, B. Ullrich, L. Grazulis, S. Elhamri, J. C. Wickett, and D. W. Stokes, J. Appl. Phys. **100**, 123110 (2006).
[8] H. J. Haugan, G. J. Brown, F. Szmulowicz, L. Grazulis, W. C. Mitchel, S. Elhamri, and W. D. Mitchel, J. Cryst. Growth **278**, 198 (2005).
[9] M. Walther, J. Schmitz, R. Rehm, S. Kopta, F. Fuchs, J. Fleißner, W. Cabanski, and J. Ziegler, J. Cryst. Growth **278**, 156 (2005).
[10] R. Kaspi, C. Moeller, A. Ongstad, M. L. Tilton, D. Gianardi, G. Dente, and P. Gopaladasu, Appl. Phys. Lett. **76**, 409 (2000).
[11] A. P. Ongstad, R. Kaspi, C. E. Moeller, M. L. Tilton, D. M. Gianardi, J. R. Chavez, and G. C. Dente, J. Appl. Phys. **89**, 2185 (2001).
[12] E. Plis, S. Annamalai, K. T. Posani, S. Krishna, R. A. Rupani, and S. Ghosh, J. Appl. Phys. **100**, 014510 (2006).
[13] Y. Wei, A. Gin, M. Razegui, and G. J. Brown, Appl. Phys. Lett. **81**, 3675 (2002).
[14] Y. Wei, A. Gin, M. Razeghi, and G. J. Brown, Appl. Phys. Lett. **80**, 3262 (2002).
[15] M. Altarelli, Phys. Rev. B **28**, 842 (1983).
[16] R. Magri, L. W. Wang, A. Zunger, I. Vurgaftman, and J. R. Meyer, Phys. Rev. B **61**, 10235 (2000).
[17] R. Magri and A. Zunger, J. Vac. Sci. Technol. B **21**, 1896 (2003).
[18] A. Zakharova, S. T. Yen, and K. A. Chao, Phys. Rev. B **64**, 235332 (2001).
[19] A. Zakharova, S. T. Yen, and K. A. Chao, Phys. Rev. B **66**, 085312 (2002).
[20] I. Lapushkin, A. Zhakarova, S. T. Yen, and K. A. Chao, J. Phys.: Condens. Matter **16**, 4677 (2004).
[21] M. J. Yang, C. H. Yang, B. R. Bennett, and B. V. Shanabrook, Phys. Rev. Lett. **78**, 4613 (1997).
[22] R. Magri and A. Zunger, Phys. Rev. B **68**, 155329 (2003).
[23] R. Magri and A. Zunger, Phys. Rev. B **65**, 165302 (2002).
[24] F. Szmulowicz, H. Haugan, and G. J. Brown, Phys. Rev. B **69**,

155321 (2004).
[25] O. Krebs and P. Voisin, Phys. Rev. Lett. **77**, 1829 (1996).
[26] S. H. Kwok, H. T. Grahn, K. Ploog, and R. Merlin, Phys. Rev. Lett. **69**, 973 (1992).
[27] H. J. Haugan, F. Szmulowicz, G. J. Brown, B. Ullrich, S. R. Munshi, L. Grazulis, K. Mahalingam, and S. T. Fenstermaker, Physica E (Amsterdam) **32**, 289 (2006).
[28] C. N. Cionca, D. A. Walko, Y. Yacoby, C. Dorin, J. Mirecki Millunchick, and R. Clarke, Phys. Rev. B **75**, 115306 (2007).
[29] R. Magri and A. Zunger, IEE Proc.-J: Optoelectron. **150**, 409 (2003).
[30] R. Magri and A. Zunger, Physica E (Amsterdam) **13**, 325 (2002).
[31] A. Zunger and A. J. Freeman, Phys. Rev. B **16**, 2901 (1977).
[32] C. Persson, A. F. da Silva, R. Ahuja, and B. Johansson, J. Cryst. Growth **231**, 397 (2001).
[33] C. Persson, B. E. Sernelius, A. F. da Silva, R. Ahuja, and B. Johansson, J. Phys.: Condens. Matter **13**, 8915 (2001).
[34] J. M. Luttinger and W. Kohn, Phys. Rev. **97**, 869 (1955).
[35] E. O. Kane, J. Phys. Chem. Solids **1**, 249 (1957).
[36] B. A. Foreman, Phys. Rev. B **72**, 165345 (2005); Phys. Rev. Lett. **86**, 2641 (2001); **81**, 425 (1998).
[37] A. Zunger, Phys. Status Solidi A **190**, 467 (2002).
[38] R. Magri and A. Zunger, Phys. Rev. B **62**, 10364 (2000).
[39] H. Fu, L.-W. Wang, and A. Zunger, Phys. Rev. B **57**, 9971 (1998).
[40] J. M. An, A. Franceschetti, S. V. Dudiy, and A. Zunger, Nano Lett. **6**, 2728 (2006).
[41] J. Kim, L.-W. Wang, and A. Zunger, Phys. Rev. B **57**, R9408 (1998).
[42] M. Grundmann, O. Stier, and D. Bimberg, Phys. Rev. B **52**, 11969 (1995).
[43] L.-W. Wang, A. J. Williamson, A. Zunger, H. Jiang, and J. Singh, Appl. Phys. Lett. **76**, 339 (2000).
[44] D. M. Wood and A. Zunger, Phys. Rev. B **53**, 7949 (1996).
[45] K. Kim, P. R. C. Kent, A. Zunger, and C. B. Geller, Phys. Rev. B **66**, 045208 (2002).
[46] G. Bester and A. Zunger, Phys. Rev. B **71**, 045318 (2005).
[47] L.-W. Wang, J. Kim, and A. Zunger, Phys. Rev. B **59**, 5678 (1999).
[48] L.-W. Wang and A. Zunger, J. Phys. Chem. B **102**, 6449 (1998).
[49] H. Fu and A. Zunger, Phys. Rev. B **57**, R15064 (1998).
[50] H. Fu, L.-W. Wang, and A. Zunger, Appl. Phys. Lett. **71**, 3433 (1997).
[51] H. Fu and A. Zunger, Phys. Rev. B **56**, 1496 (1997).
[52] E. L. Ivchenko, A. Yu. Kaminski, and U. Rössler, Phys. Rev. B **54**, 5852 (1996).
[53] P. Keating, Phys. Rev. **145**, 637 (1966).
[54] J. L. Martins and A. Zunger, Phys. Rev. B **30**, 6217 (1984).
[55] J. E. Bernard and A. Zunger, Appl. Phys. Lett. **65**, 165 (1994).
[56] A. Silverman, A. Zunger, R. Kalish, and J. Adler, J. Phys.: Condens. Matter **7**, 1167 (1995).
[57] L. Bellaiche, S-H. Wei, and A. Zunger, Phys. Rev. B **56**, 10233 (1997).
[58] *Numerical Data and Functional Relationships in Science and Technology*, Landolt-Börnstein Vol. 22a (Springer-Verlag, Berlin, 1987).
[59] L. Hedin, J. Phys.: Condens. Matter **11**, R489 (1999).
[60] L. W. Wang and A. Zunger, J. Chem. Phys. **100**, 2394 (1994).
[61] M. J. Yang, W. J. Moore, B. R. Bennett, B. V. Shanabrook, J. O. Cross, W. W. Bewley, C. L. Felix, I. Vurgaftman, and J. R. Meyer, J. Appl. Phys. **86**, 1796 (1999).
[62] O. Dehaese, X. Wallart, and F. Mollot, Appl. Phys. Lett. **66**, 52 (1995).
[63] Futher details on the calculation of the exchange probabilities and on the specific values used for the deposition rates are found in Ref. 23.